Computer simulation of nanoindentation into polymer films

Gerald Pätzold, Andreas Linke, Thorsten Hapke, and Dieter W. Heermann*
Institut für Theoretische Physik, Universität Heidelberg,
Philosophenweg 19, D-69120 Heidelberg, Germany and
Interdisziplinäres Zentrum für wissenschaftliches Rechnen der Universität Heidelberg
(January 16, 1997)

Abstract

We report on computer experiments of nanoindentation into amorphous polymer films. The bulk polymer is described by a united atom model in connection with molecular dynamics methods. The interaction between the indenting tool and the polymer is purely repulsive. The dynamics of the tool is modeled as overdamped, such that the indentation velocity is proportional to the difference between the external force acting onto the tool and the resistance force built up in the polymer film. We concentrate on the initial, kinetic stage of the indentation process and give results for the motion of the indenting blade, the deformation field of the polymer film, the stress field, and the fields of monomer density and energy. We derive an effective coefficient as a new measure for the resistivity of a surface against indentation. Its value can be determined in an experiment with constant indentation velocity. In addition, we investigate the free drift behavior after the external driving force has been set to zero and the tool is expelled from the polymer film. For different polymer chain lengths, the tool's motion is exponential in time and we determine the relevant relaxation times. We address the resistance of the film, its surface hardness, local deformation mechanisms during indentation, and recovery phenomena in amorphous materials. Visualizations of various issues discussed in the paper may be found on one of our web pages, see `http://wwwcp.tphys.uni-heidelberg.de/~paetzold/`.

Keywords: nanoindentation, thin amorphous polymer films, computer simulation, resistance and recovery of amorphous materials

68.60.Bs, 81.40.Lm, 81.40.Pq

Typeset using REVTEX

*Contact: `heermann@tphys.uni-heidelberg.de`, `http://wwwcp.tphys.uni-heidelberg.de/`

I. INTRODUCTION

The penetration of a sharp body into a surface is one of the most basic damage and testing mechanisms one can think of. We study this situation for the case of a rigid tool which indents a thin amorphous polymer film. The film can be thought of as some representative component for micro- or even nanotechnological design. Moreover, thin films are studied on their own right. They vary in thickness from tens of nanometers to micrometers. Important applications include resists and interlayer dielectrics in microelectronics fabrication, alignment layers in liquid crystal displays, lubricants in magnetic information storage devices, and coatings for wear protection and corrosion [1]. In most cases, the material of the film is chosen for its functional property (electronic, magnetic, or optical). For other miniaturized components, Young's modulus is the most important material property, because the operational principle of many micromechanical components is based on the elastic behavior of the material. Examples for such components are pressure sensors in which a membrane is deflected by an applied pressure, or acceleration sensors, in which a seismic mass is deflected by an applied acceleration.

In many applications, the microscopic components are expected to withstand harsh mechanical influences. Several factors can cause mechanical stresses, which results in various deformation and fracture phenomena. Thus, besides the functional properties, also the mechanical properties are of importance for the desired function of thin films. Many mechanical testing methods applied to macroscopic bulk materials can obviously not be used for films less than a micron thick. Special care has to be taken to measure the properties of the film and not of the substrate. Much work has been spent to the development of reliable and accurate techniques to measure the elastic properties (Young's modulus), stresses, adhesion, hardness, and fracture resistance of thin films.

Despite the importance of Young's modulus, the often well known values were obtained from macroscopic specimens. They cannot be transferred to smaller scales, since the elastic behavior of miniaturized components can differ significantly from the elastic behavior of their everyday-size counterparts. For crystalline solids, reasons for this difference are well known and can be attributed to the increasing role of residual stresses in small components, the increasing ratio of surface to volume with decreasing component size, differences in the microstructure, e.g. the grain size, of the material, and geometric nonlinearities, which occur frequently in microsized components. Thus, Young's modulus has to be determined directly from specimens of the original size, which requires the development of special testing techniques. For amorphous solids such as polymers, additional complications arise, e.g. from the glassy nature of the materials.

One feasible testing technique is nanoindentation. It is similar to conventional hardness testing, but is performed on a much smaller scale. In the basic experimental setup, the force required to press a sharp diamond indenter into a material is measured as a function of the indentation depth. The experimental depth resolution on the scale of nanometers allows nowadays to conduct indentation experiments even on very thin films. Two quantities which can be readily extracted from nanoindentation experiments are the Young's modulus, i.e. the material's stiffness, and the hardness, which can be correlated to yield strength [2]. Nanoindentation experiments have also been used to study creep, plastic flow, and fracture of materials. Experimental nanoindentation depends on a number of parameters, like the shape

of the indenter tip and the strain history of the sample. The latter affects the material's structure and can lead to strain hardening and a change in the measured results.

A related issue is to enhance the understanding of the deformation behavior of thin films at elevated processing temperatures and to develop thermal-mechanical models. For example, typical processing temperatures for polymer films range from 400 to 600 Celsius degrees. The deformation of amorphous thin films then consists of elastic and viscous parts. The viscous flow can be described by suitable mechanical models based on additional material properties such as the viscosity. The viscosity is usually a function of temperature and stress, and has a strong dependence on microstructure and composition. An important parameter in the indentation process is then also the indentation velocity. Dependent on its magnitude, one can distinguish between quasistatic indentation (where the film material retains its equilibrium properties) and out-of-equilibrium indentation. We here consider the latter regime. If the indenter's velocity is comparable to the film material's speed of sound, effects of compressibility such as fluctuations in the mass density are observed.

Luedtke and Landman [3] performed computer experiments to study the formation of solid junctions between metal surfaces and metal tips, and of liquid junctions between metal tips and hexadecane molecules. Part of their motivation was to contrast continuum based contact mechanics with atomistic simulations. These authors stress that nanoindentation can not only be used to probe materials but also to induce atomic-scale structural modifications via tip substrate interactions. They envisage purposeful manipulations and the nanostructural design of surfaces. Our approach and methodology is similar to that of Luedtke and Landman. The most fundamental quantity they monitored is the tip's position during the simulation and the associated energy. They included the attractive part of the tip/surface interaction potential; therefore they observed adhesion and the jump-to-contact instability. This is not the case in our study. Our interest goes into the displacement of matter during indentation and we avoid the peculiarities of detailed metal/polymer interaction potentials. The generic repelling potential we use allows us to study the kinematics of the deformation field and the stress response.

Recently, nanoindentation into polymer surfaces has further been studied experimentally [4]: an atomic force microscope was used in force mode to investigate the mechanical behavior of polyurethane and epoxy samples under mechanical load. The AFM probe tip was first lowered into contact with the sample, then indented into the surface, and finally lifted off of the sample surface. Indepently, we decided to look at the relaxation behavior after the forced indentation in computer simulations, too. Several microindentation studies [5] have revealed the importance of the slope of the load-penetration curve or contact stiffness,

$$s = \frac{\partial F_{\text{external}}}{\partial z_{\text{tool}}} = \frac{2rE}{1-\nu^2}\,, \tag{1}$$

where F_{external} is the indentation load, z_{tool} is the penetration depth, r is the contact radius, and E and ν are the sample elastic modulus and Poisson's ratio, respectively. The second equality follows from pure elastic Hertzian (spherical tip into plane surface) contact theory [6]. It neglects any nonreversible, plastic deformations and is thus applicable only for limited indentation depths. For the ductile, amorphous polymers under consideration here, this theory can only give some guidance how to proceed in a more general case.

Again assuming that the unloading process is characterized by elastic recovery only, the indentation displacement, $z_{\rm tool}$, can be related to the applied force, $F_{\rm external}$, by the following equation generally attibuted to Sneddon [7],

$$F_{\rm external} = \frac{\xi E}{1-\nu^2} z_{\rm tool}^m \,, \tag{2}$$

where ξ is a constant wich depends on the geometry of the contact. The exponent m is characteristic of the geometry of indentation during unloading. The unloading geometry does not, in general, correspond to the indenter geometry because of plastic deformation in the vicinity of the indenter tip created during the loading process. This plastic deformation, along with the indenter geometry, determines the effective shape of indentation during unloading.

For the polyurethane samples in Ref. [4], large amounts of elastic deformation, as measured from the unloading response, were observed, and the amount of inelastic deformation, as measured by the hysteresis between the load and unload curves, depended on the magnitude of the maximum load. For samples with different values of Young's modulus, quite similar values of $m = 1.54 \ldots 1.56$ were observed, indicating similar unloading geometries. But the total amout of indentation, as well as the amounts of elastic deformation and load-unload hysteresis, is larger for the lower modulus material. This observation indicates that for these materials, as the penetration depth increases, the deformation zone increases such that both elastic and inelastic deformations increase.

In the next section, we give a short review about the simulation model we use. ... Previous results with an emphasis on the overall deformation characteristics rather than on the more local effects considered here have already been published [8].

II. POLYMER MODEL, SIMULATION METHOD, AND POSTPROCESSING

A. United atom model for polyethylene

For the polymer chains, we use a united atom model in conjunction with Newtonian dynamics. In addition to harmonic chain forces which keep the bond lengths next to the equilibrium value, we model the fluctuation of bond angles, again by a quadratic potential. Between monomers which do not participate in mutual bond length or bond angle interactions, Lennard-Jones forces are acting, both to model an excluded volume effect and to hold the polymer system together. Note that, for the sake of simplicity, we neglect any torsion potential in the present study. Future work will address more detailed potentials and elaborate polymer models. Here we use a generic model for chain molecules with only a small number of adjustable parameters. The Hamiltonian of the present model is thus

$$\begin{aligned} H &= H_{\rm bondlength} + H_{\rm bondangle} + H_{\rm LJ} \,, \\ H_{\rm bondlength} &= \sum_{\rm bonds} \frac{k_b}{2} \left(l_{\rm bond} - l_0 \right)^2 \,, \\ H_{\rm bondangle} &= \sum_{\rm angles} \frac{k_\theta}{2} \left(\cos\theta_{\rm angle} - \cos\theta_0 \right)^2 \,, \end{aligned} \tag{3}$$

TABLE I. Parameters of the polyethylene model.

Lennard-Jones energy, ϵ	$8.3027 \cdot 10^{-22}$ J	500 J/mol
Lennard-Jones length, σ	380 pm	3.8 Å
monomer mass (CH_2 group), m	$2.3248 \cdot 10^{-26}$ kg	14 atomic units
temperature, T	361 K	
bond length, l_0	152 pm	1.52 Å
bond angle, θ_0	109.47°	$\cos\theta_0 = -1/3$
spring constant (bond length), k_b	$5.7498 \cdot 10^{1}$ N/m	$3.46 \cdot 10^{7}$ J/(nm^{2}mol)
bending constant (bond angle), k_θ	$8.3027 \cdot 10^{-19}$ J	$5 \cdot 10^{5}$ J/mol
simulation time step, Δt	2.0108 fs	

$$H_{\mathrm{LJ}} = \sum_{\substack{\text{pairs of}\\ \text{monomers}}} 4\epsilon \left[\left(\frac{\sigma}{r_{\mathrm{pair}}} \right)^{12} - \left(\frac{\sigma}{r_{\mathrm{pair}}} \right)^{6} \right] .$$

The Lennard-Jones interaction is implemented with a cutoff of $2.5\,\sigma$ and appropriate potential and force shifts are used to retain continuity. We use molecular dynamics methods to compute the motion of the monomers. Models of this kind are described at various places in the literature [9]. We intend to capture some essential features of polyethylene chains and appropriate model parameters are compiled in Tab. I (see also Ref. [10]). The preparation and the properties of free polymer surfaces for this model have already been discussed by us [11].

B. Details of the simulation procedure

The setup and computer implementation of the blade indentation experiment has been discussed at length in Ref. [8]. A sketchy overview is given in Fig. 1. In the present study, the indenter is a prismatic blade and we use the neutral y-direction for additional averaging. In a forthcoming paper [12], we will report on results with a rotionally symmetric indenter. The simulations were performed at a reduced temperature of $T^* = T/(\epsilon/k_{\mathrm{B}}) = 6.0$ or a physical temperature of $T \approx 360\mathrm{K} \approx 90\,^{\circ}\mathrm{C}$. We stress that our simulations are not meant to fully mimic real polyethylene (it has been demonstrated, however, that much can be achieved by carefully tuning the parameters of united atom models [10]). The chain lengths are too short and we treat chain-end monomers like mid-chain monomers. We also neglect the torsional potential (the rotation about C-C axes is not restricted). The high temperature helps to ensure that in feasible simulation times, the chains travel several radii of gyration. We have simulated chains of length N=20, 40, and 60. The film thickness is on average 75 Å. The boundary conditions are periodic in the lateral (x and y) directions, but there is naturally no periodicity along the film thickness (z) direction. For the time integration, we use the velocity variant of the Verlet algorithm. To keep the temperature constant (indenting the tool adds work to the system and would increase the temperature), a Hoover thermostat is employed. We report on relatively short molecular dynamics run with a duration of about 20 picoseconds. The reason is that we want achieve high temporal resolution for the indentation process. To use our resources adequately, we sample polymer

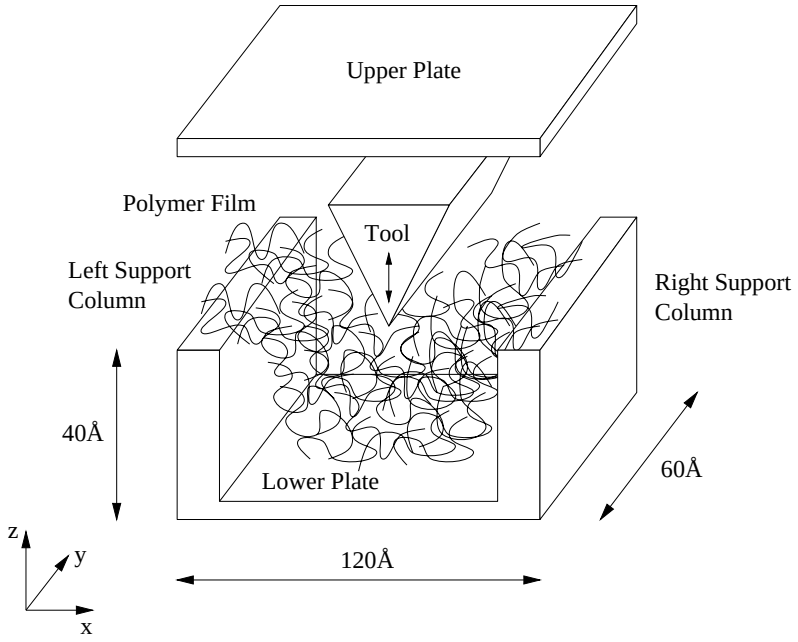

FIG. 1. Sketch of the blade indentation experiment (lengths in Å).

configurations every 0.2 picoseconds over 5 independent runs for each computer experiment. For the motion of the tool, we use overdamped dynamics,

$$v_{\text{tool}} = \frac{1}{\zeta} \left(F_{\text{external}} - F_{\text{polymer}} \right) , \tag{4}$$

where v_{tool} is the z component of the indentation velocity (motion into the x and y directions is suppressed), ζ is an adjustable friction coefficient, F_{external} is the external driving force, and F_{polymer} is the reaction force of the polymer film. The reason to use this artificial first order dynamics instead of the physical second order Newtonian dynamics for the indenter is to avoid transient phenomena. Earlier studies with Newtonian dynamics have shown that the tool undergoes damped oscillations after impact on the film. From the present study, we excluded this effect since it depends on the more or less arbitrary tool mass. The friction constant ζ in the overdamped dynamics merely sets the time scale of the indentation process. We claim that there is a regime in nanoindentation which is not governed by the inertia of the tool and for which the equilibrium condition, i.e. zero net force, is the same for first and second order dynamics.

C. Interpreting the results

Under the action of the indenting tool, the polymer film undergoes considerable deformations, at least in some active region next to the impact zone. In continuum mechanics, the deformation state is encoded into a three-dimensional vector field which describes the motion of so-called material points. In the context of particle based simulations, a first question to address is how to eventually define such points. Possible candidates are monomer

or chain center of mass coordinates. However, on the nano-scale, diffusive motion takes place. From the simulations, we know that the average free diffusive motion of monomers is 5 to 6 Å during the chosen indentation interval of 10 picoseconds. On the other hand, we observe a trend for the indenting blade to displace entire chains. But in the simulations to be presented here, there is an overlap between the linear dimensions of the tool and the chain radius of gyration. We accordingly have no seperation of scales and observations based solely on center of mass coordines of chains turn out to be too coarse. *We therefore interpret the average motion of monomers as the displacement of material points in a corresponding field description.*

In particular, we divide the volume of the polymer film into a number of subvolumes. A first average deformation is then computed from all monomers in each subvolume. The information gained is associated with the geometrical center of the subvolume. In addition, statistics over several independent simulation runs is performed. Again, the key assumption is that the average particle motion (computed as the arithmetic mean) is amenable to a continuous field description. When contour lines, e.g. of the total displacement field, have to be computed, one better smears out steep gradients by use of a low pass filter (weighted average over nine neighbour points). It may be necessary to use additional interpolation or approximation algorithms when it comes to the computation of derived quantities like the deformation gradient field. Finally, in addition to the motion of points, it may be of advantage to follow the motion of other geometric primitives (lines, surfaces, or subvolumes spanned by certain monomers) in order to characterize the deformation process.

An analogous approach is used to compute stress fields. The expression [13]

$$\sigma_{\alpha\beta} = -\frac{1}{V}\sum_{m} \langle F_{m\alpha} R_{m\beta} \rangle \tag{5}$$

is evaluated in subvolumes V, $F_{m\alpha}$ is the force onto monomer m into coordinate direction α, $R_{m\beta}$ is the β-component of the position vector of that monomer. In practice, we compute the contributions to the foregoing formula arising from interactions between pairs and triples of monomers. We then determine the common center of mass of the participating monomers and use this position to sort the contribution into the subvolume bins. In the present study, we do not consider the question if stresses are mediated mainly by Lennard-Jones (or, in general, interchain) interactions or if the polymer backbone (intrachain interactions) plays the essential role.

According to the geometry of the blade indentation experiment, one might first be tempted to describe the film deformation as *bending*. We have suggested the term "polymer film bending" before [8]. However, "bending" is quite a technical term [14]. The simplest theory deals with an idealized model of a cantilever beam, the "Bernoulli beam", which is characterized by two assumptions, (1) that plane cross sections remain plane during the bending process, and (2) that cross sections remain perpendicular to the neutral axis of the beam. The neutral axis connects all the centers of cross section. We do of course not assume that our polymer film deforms like a purely elastic Bernoulli beam. But there are two general signatures of bending deformation which can be looked for in the simulation results, (1) some neutral axis or plane can be identified which is characterized by zero strain, (2) the neutral axis separates regions of pressure and tension, i.e. to both sides of the neutral plane in the polymer film we find stresses of opposite sign.

Under the action of the load applied to the film, *shear* deformation has to be expected, too. This is especially the case since the polymer melt we simulate is quite liquid in nature and can hardly withstand any shearing forces. However, it will turn out that on the time scale accesible to our simulations, the deformations are quite local and restricted to the *impact zone*. This can be seen by computing characteristic invariants from deformation and stress fields which also allow to distinguish between the different types of deformation. Doing so, we cannot identify extended shearing planes.

III. FORCED INDENTATION AND EFFECTIVE RESISTANCE COEFFICIENT

For each polymer chain length (N=20, 40, and 60), the raw data for the tip movement during forced indentation and free drift have been obtained as an average over 5 independent runs. Fig. 2 shows the curves for blade position vs. time for N=40 ("0" on the blade position axis indicates the position of the film's upper surface). At the very beginning, there is no appreciable interaction between the blade and the film. According to the overdamped dynamics, the blade moves downward very quickly. These first 100 femtoseconds are not properly resolved in the figure. The comparison between the absolute indentation depths resulting from this initial phase for different chain lengths is problematic. We found an increase in depth going from N=20 to N=40, but for N=60, the indentation is smaller again. We feel that to clarify this issue, more simulations with better time resolution of the startup phase have to be performed. It may well be that the missing unique trend in the present result is an artifact of some overshoot effect.

However, with the exception of this very short startup phase, the indenter moves downwards with nearly constant velocity. Referring to Eqn. (4), this means that the reaction force emerging from the polymer film, F_{polymer}, is constant in time. This is a remarkable result, since the reaction force is the sum of all polymer/tool interactions, and due to indentation, an ever increasing area of the tool dips into the film. – The maximum indentation depth after 10 picoseconds, about 25 Å, should be compared to the film thickness of 75 Å.

Sample polymer configurations resulting from the indentation simulations were stored after 2, 4, 6, 8, and 10 picoseconds. These configurations were then used to start the simulation program again, but with the external force onto the tool set to zero. The tool is then pushed out of the film. These free drift curves show the signature of a relaxation process and are further analyzed below.

The indentation curve in Fig. 2 corresponds to an external force of 1.0 nano Newton. In Fig. 3 then, curves for different chain length as well as for different external forces are plotted. In order to compare their slope (we have mentioned above that it is problematic to do this for the absolute indentation depth), the curves have been shifted such that they all pass through blade position $z_{\text{tool}} = 0$ at $t = 2$ picoseconds. In Tab. II, the net forces onto the tool,

$$F_{\text{net}} = F_{\text{external}} - F_{\text{polymer}} \,, \tag{6}$$

are compiled for different chain length and external driving forces F_{external}. These quantities have been sampled during the simulation runs and can in turn be used to compute the

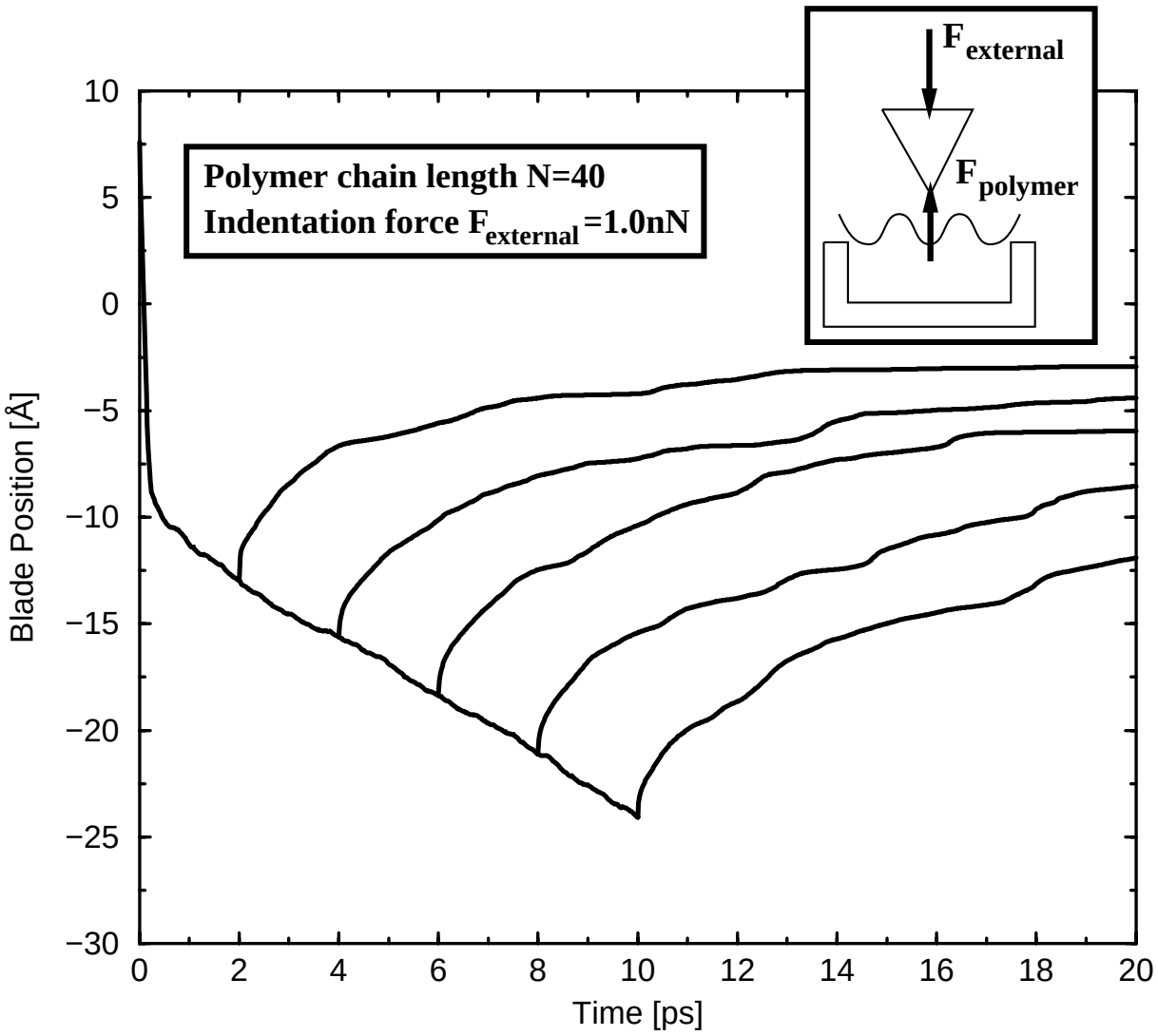

FIG. 2. Indentation and free drift curves with chain length N=40 and indentation force $F_{\text{external}} = 1.0$ nN. During the indentation process, both F_{external} and F_{polymer} are different from zero. For the free drift experiments, $F_{\text{exertanal}}$ has been set to zero.

TABLE II. Tool net forces $F_{\text{net}} = F_{\text{external}} - F_{\text{polymer}}$ and indentation velocities v_{tool}. For each external force, the first column gives the mean net force onto the tool (in pico Newton) as measured in the simulation. The second column is the estimated tool velocity, calculated with the friction coefficient of $\zeta = 11.56$ pN/(Å/ps). The third column is the actual indentation velocity as given by the slope of the linear fit to the indentation curves (both velocities in Å/ps, where 1 Å/ps = 360 km/h).

Chain length	$F_{\text{external}} = 1.0$ nN			$F_{\text{external}} = 1.5$ nN			$F_{\text{external}} = 2.0$ nN		
20	-15.5086	-1.34	-1.30	-23.9275	-2.07	-2.12	-29.7333	-2.57	-2.61
40	-15.9768	-1.38	-1.35	-21.3637	-1.85	-1.87	-26.5775	-2.30	-2.31
60	-14.5866	-1.26	-1.22	-19.8963	-1.72	-1.75	-24.1507	-2.09	-2.07

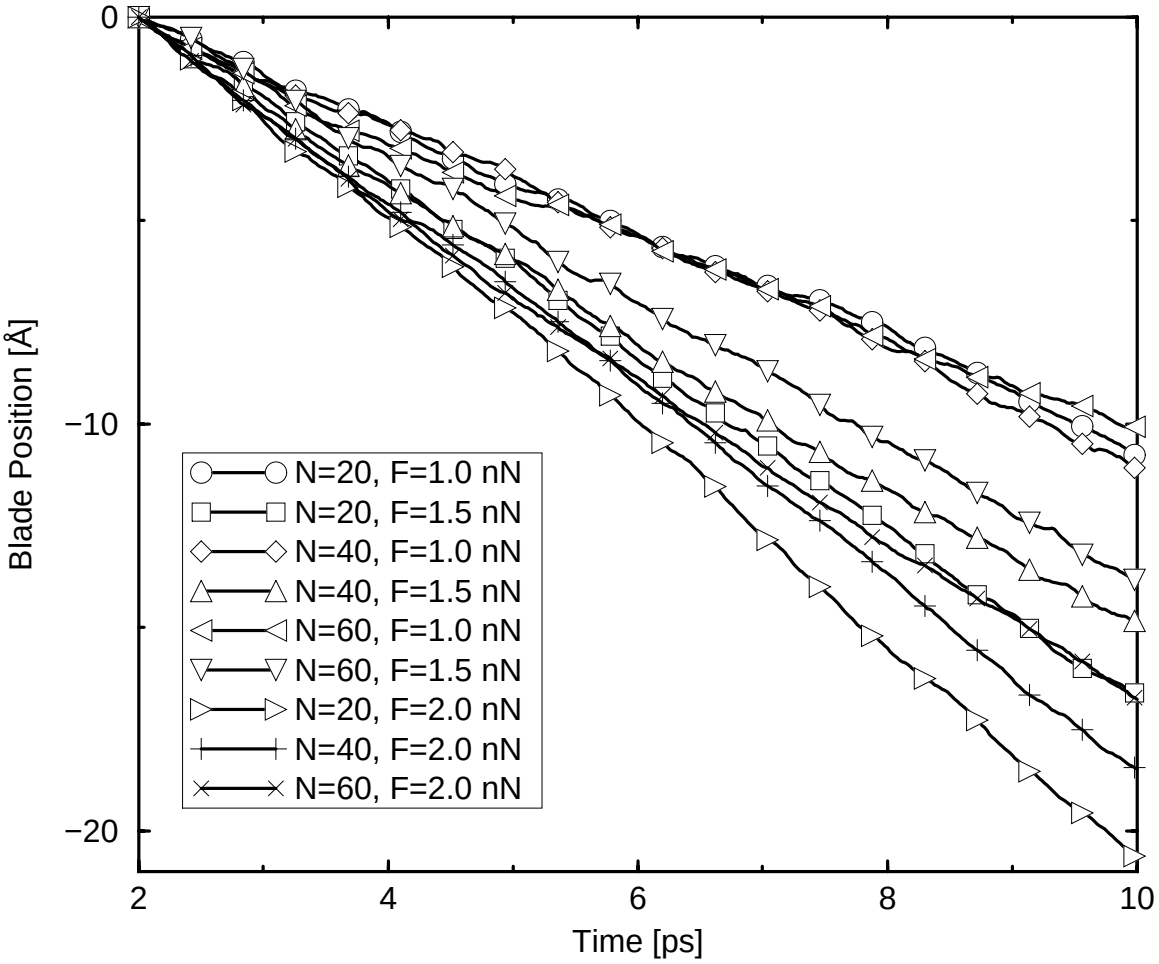

FIG. 3. Tool indentation curves for chain length $N = 20$, 40, and 60, and indentation forces F_{external} of 1.0, 1.5, and 2.0 nN.

TABLE III. Reaction forces F_{polymer} in the polymer film (in pico Newton).

Chain length	$F_{\text{external}} = 1.0$ nN	$F_{\text{external}} = 1.5$ nN	$F_{\text{external}} = 2.0$ nN
20	984.49	1476.07	1970.27
40	984.02	1478.64	1973.42
60	985.41	1480.10	1975.85

TABLE IV. Effective resistance coefficients (in pN/(Å/ps)).

Chain length	$F_{\text{external}} = 1.0$ nN	$F_{\text{external}} = 1.5$ nN	$F_{\text{external}} = 2.0$ nN
20	729.93	707.55	766.28
40	740.74	802.14	865.80
60	819.67	857.14	966.18

reaction force F_{polymer} in the polymer film as summarized in Tab. III. In Tab. II also the tool velocities calculated according to (cf. Eqn. (4)),

$$v_{\text{tool}} = F_{\text{net}}/\zeta \,, \tag{7}$$

and the tool velocities as determined from linear fits for the the curves in Fig. 3 are given. The deviations of a few percent are attributed to numerical inaccuracies and cumulative errors during the data sampling.

In Tab. IV, the effective resistance coefficients, defined as

$$\zeta_{\text{eff}} = F_{\text{external}}/v_{\text{tool}} \,, \tag{8}$$

are given. These quantities relate the applied external force to the observed velocity. *We claim that this effective coefficient is an appropriate measure for a material's resistivity against indentation. The effective resistance coefficient provides a dynamical characteristic for the surface hardness.* Fig. 4 shows the data from Tab. IV plotted vs. the chain length. The effective resistance coefficient is a material property, but not a material constant. This non-linear behavior can clearly be seen in Fig. 5, where the coefficient is plotted against the driving force, F_{external}. For higher external driving (and higher indentation velocity, cf. Tab. II), the coefficient increases.

IV. FREE DRIFT AND CHARACTERISTIC RELAXATION TIMES

For each chain length, the five free drift curves as in Fig. 2 were shifted in such a way that the first data points come to the origin of the coordinate system. It then turns out that the shifted curves can be fitted to functions of the form

$$f(t) = A(1 - \exp(t/\tau)) \,. \tag{9}$$

The relaxation times τ show no clear dependence on the indentation depth where the tool was released (i.e. after 2, 4, 6, 8, or 10 picoseconds). Therefore, for each chain length, an average relaxation time as plotted in Fig. 6 was computed. *The time scale τ is characteristic for the recovery phenomena in the amorphous polymer film. The determination of τ gives information about how fast surface damages on the nano-scale heal.*

Up to this point, the mean properties of free drift processes, as determined from averaging over a number of independent simulation runs, have been discussed. A more detailled picture arises if one looks at the free drift dynamics of a single run. This is shown in Fig. 7 for chains with N=40. The external tool indentation force of initially 1.0 nano Newton was set

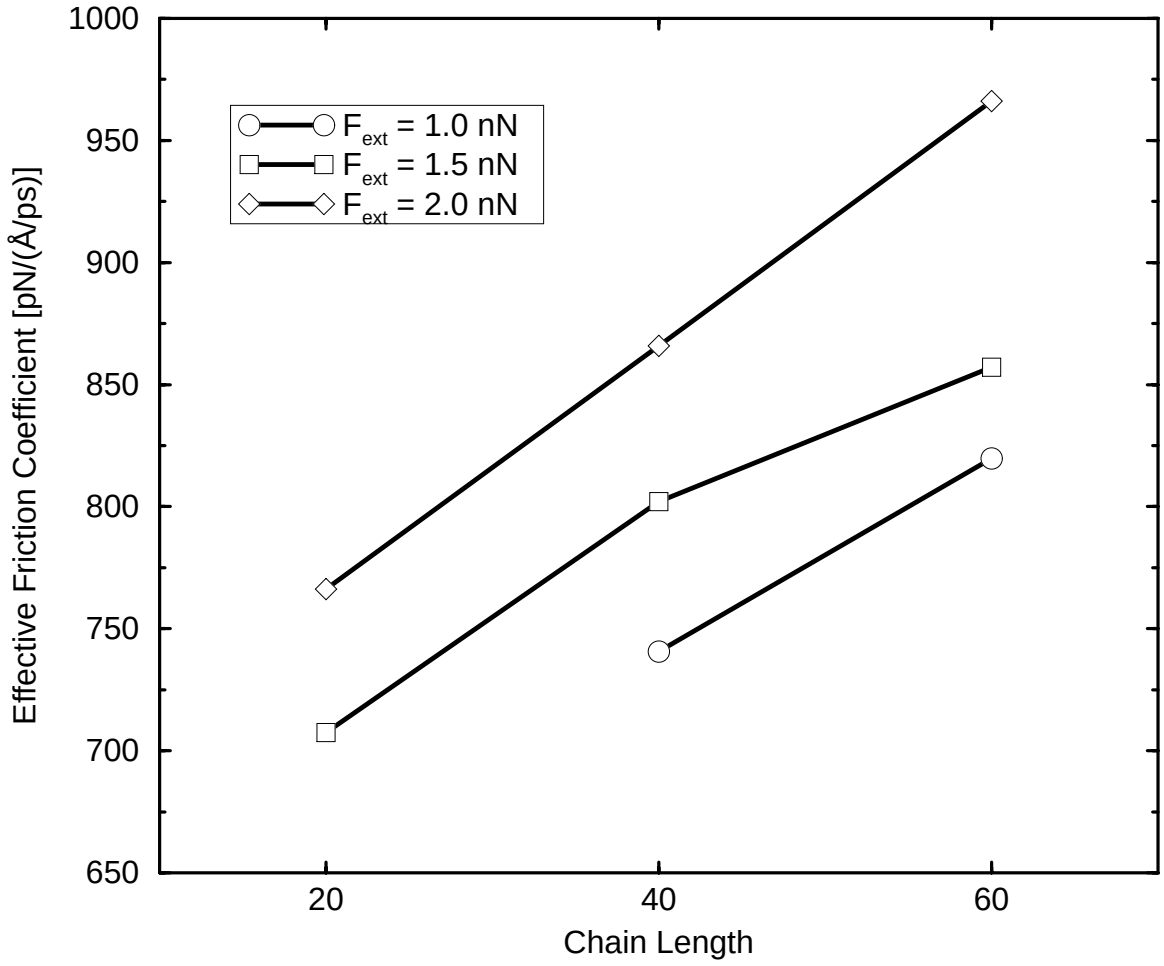

FIG. 4. Chain length dependence of the effective resistance coefficients. The result for $N = 20$ and $F_{\mathrm{external}} = 1.0$ nN is spoiled by finite chain length effects and omitted from the plot.

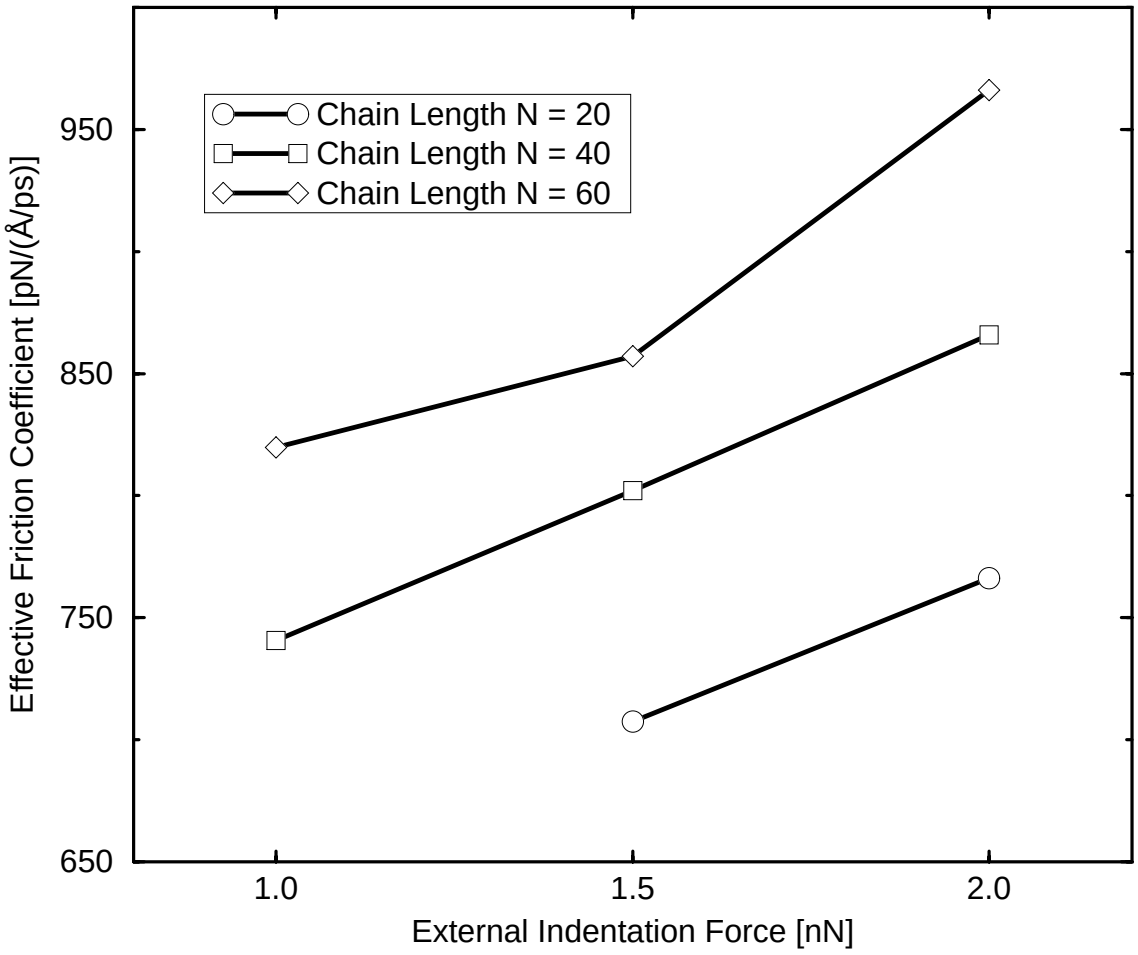

FIG. 5. Force dependence of the effective resistance coefficients. The result for $N = 20$ and $F_{\mathrm{external}} = 1.0$ nN is spoiled by finite chain length effects and omitted from the plot.

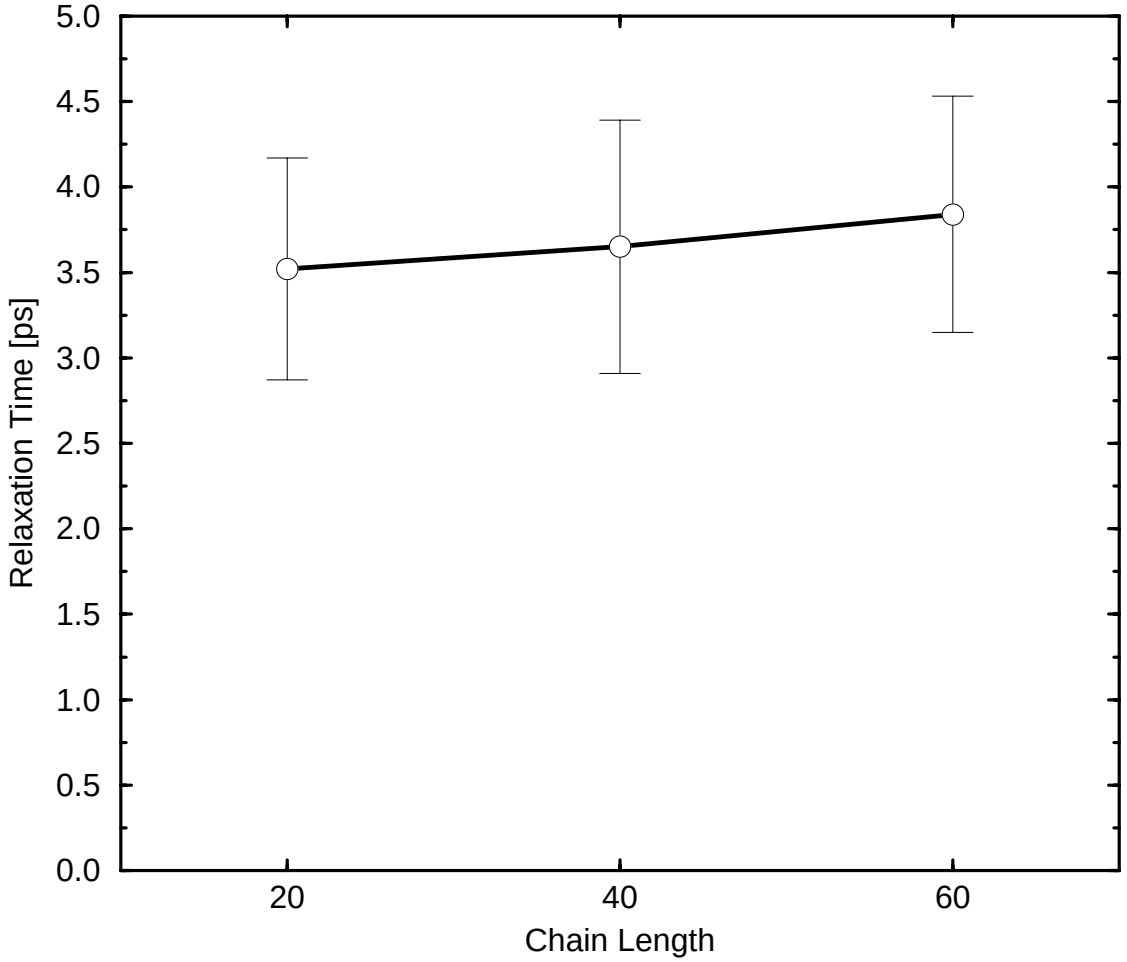

FIG. 6. Relaxation times for different chain lengths. The data for the figure are N=20: $\tau = 3.52 \pm 0.65$ ps, N=40: $\tau = 3.65 \pm 0.74$ ps, N=60: $\tau = 3.84 \pm 0.69$ ps.

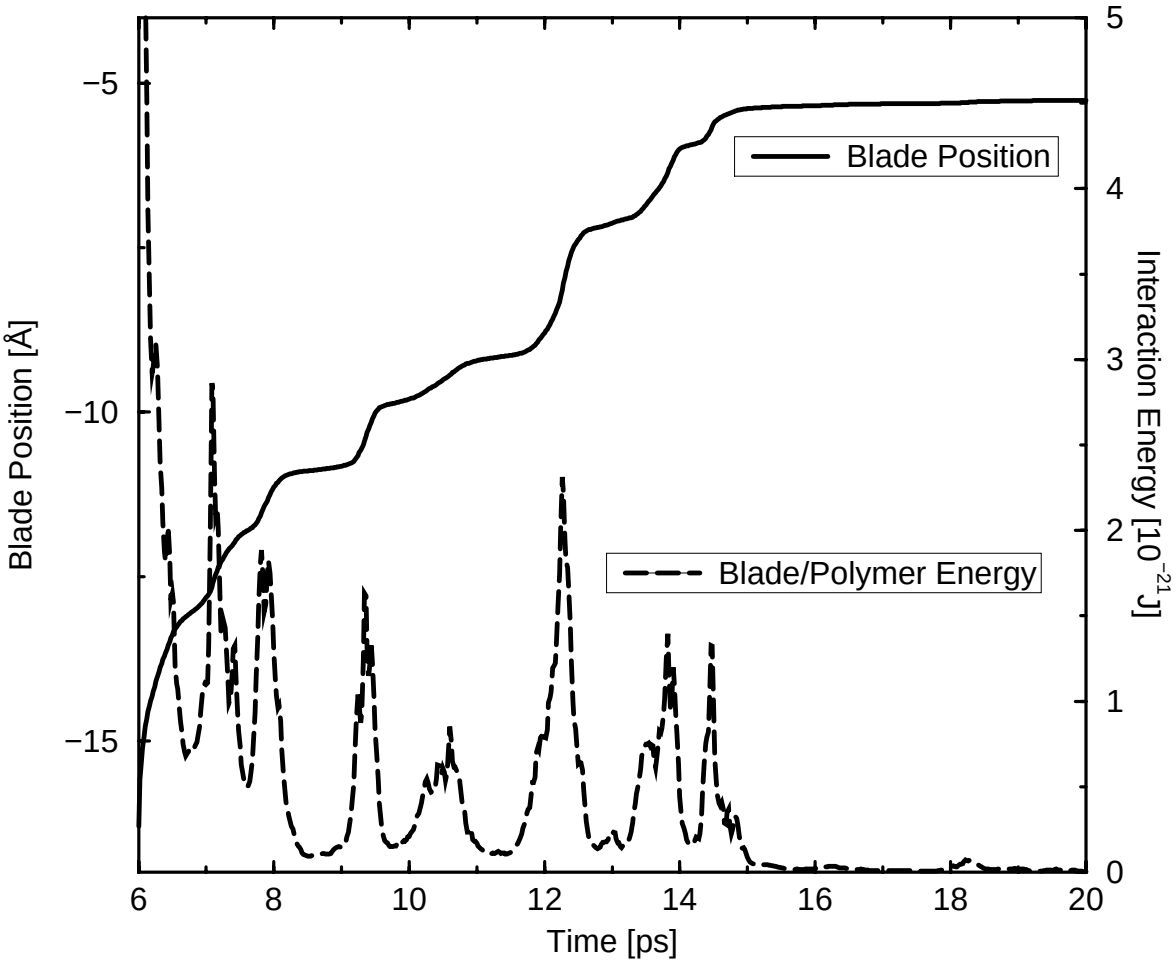

FIG. 7. Free drift dynamics of a single polymer configuration. Shown are the blade position and the tool/polymer interaction energy.

to zero after 6 picoseconds. The displacement of the tool from the polymer film is not a continuous process but happens to be a sequence of discrete events which show up as steps in the position curve and as sharp maxima in the tool/polymer interaction energy. To identify these elementary events and the underlying mechanism on the scale of monomers will be a demanding exercise in the three dimensional visualization of polymer configurations which we hope to accomplish in the next future.

V. LOCAL DEFORMATION, STRESS AND ENERGY FIELDS

The foregoing analysis of the blade indentation simulations was restricted to *global* properties. By this we mean the behavior due to cumulative effects stemmig from all polymer chains in the film. The motion of the indenter certainly reflects the interaction of large numbers of monomers. In what follows, we want to take a closer look and present the *local* deformation, stress, and energy fields. As discussed above, these fields have been computed as subvolume averages over stored polymer configuration files.

A. Total displacement fields

We first turn to an invariant of the deformation field. The displacement vector field is based on the motion of single monomers. The *scalar field of total displacement* is then defined as the length of the displacement vectors,

$$d(\mathbf{x}, t) = |\mathbf{x}(\boldsymbol{\xi}, t) - \boldsymbol{\xi}| \,. \tag{10}$$

Here $\boldsymbol{\xi}$ is the reference position of each control volume at the beginnig of the simulation and $\mathbf{x}(\boldsymbol{\xi}, t)$ is the average position at time t of all monomers initially in that volume. Note that the field values have been plotted at the positions $\mathbf{x}$ after deformation, not at the initial reference positions $\boldsymbol{\xi}$. Fig. 8 shows a time sequence of isocontour lines for the total displacement field. One clearly observes a spreading impact zone. On the other hand, after 10 picoseconds, a great part of the film is not affected by the indentation process (enclosed by the 6 Å line). Also note the region of enhanced displacement at the bottom of the film opposite to the indentation notch.

VI. CONCLUSION AND OUTLOOK

We have looked in some detail onto the behavior of polymer films under local disturbances caused by an indenting tool. New and interesting behavior on the nano-scale could be observed.

ACKNOWLEDGMENTS

This work is supported by the Bundesministerium für Bildung und Forschung (BMBF) in the framework of the project "Computersimulation komplexer Materialien" under grant no. 03N8008D.

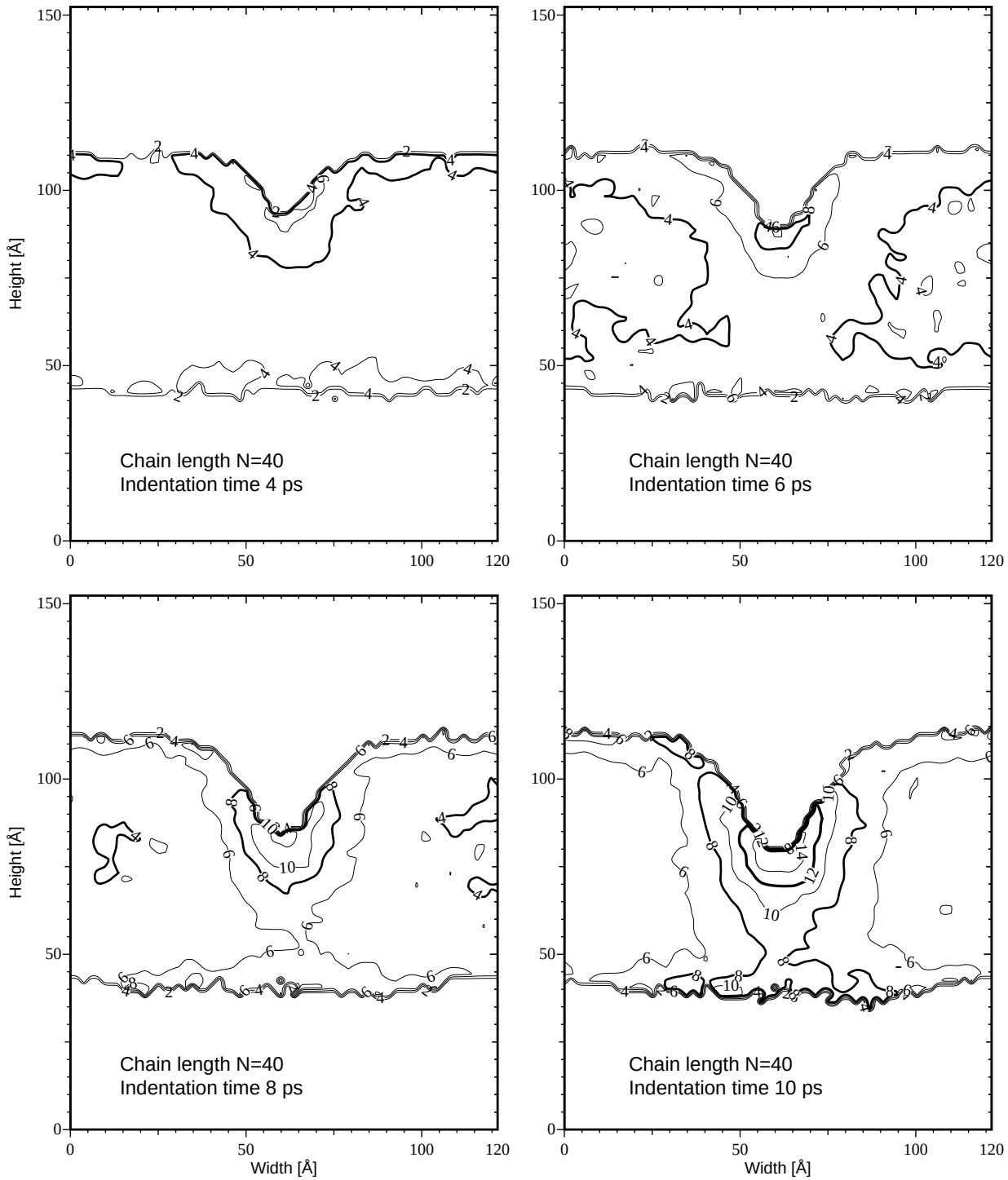

FIG. 8. Isocontour lines (labels in Å) of the total displacement field. The time sequence shows how the disturbance caused by the indenter spreads out (indentation force $F_{\text{external}} = 2.0$ nN, chain length N=40).

REFERENCES

[1] C. W. Frank *et al.*, Science **273**, 912 (1996).

[2] M. F. Doerner and W. D. Nix, J. Mater. Res. **1**, 601 (1986); T. P. Weihs, S. Hong, J. C. Bravman, and W. D. Nix, J. Mater. Res. **5**, 931 (1988); Mater. Res. Symp. Proc. **130**, 87 (1989); W. D. Nix, Metall. Trans. **20A**, 2217 (1989); J. J. Vlassak and W. D. Nix, Phil. Mag. **A67**, 1045 (1993); J. Mech. Phys. Solids **42**, 1223 (1994); R. P. Vinci and J. J. Vlassak, Annu. Rev. Mater. Sci. **26**, 431 (1996).

[3] W. D. Luedtke and U. Landman, Comp. Mat. Sci. **1**, 1 (1992).

[4] M. R. Vanlandingham *et al.*, *Relating polymer indentation behavior to elastic modulus using atomic force microscopy*, contribution Ca9.13 to the MRS 1996 fall meeting, December 2-6, Boston, Massachusetts (symposium Ca: structure and evolution of surfaces).

[5] J. B. Pethica and W. C. Oliver, Physica Scripta **T19**, 61 (1987); W. C. Oliver and G. M. Pharr, J. Mater. Res. **7**, 1564 (1992); S. P. Jarvis, T. P. Weihs, A. Oral, and J. B. Pethica in *Thin Films: Stresses and Mechanical Properties IV*, edited by P. H. Townsend (Mater. Res. Soc. Proc. **308**, Pittsburgh, PA, 1993), pp. 127-132.

[6] S. P. Timoshenko and J. N. Goodier, *Theory of Elasticity* (McGraw-Hill, New York, 1970), chapter 12.

[7] I. N. Sneddon, Int. J. Eng. Sci. **3**, 47 (1965).

[8] G. Pätzold, T. Hapke, A. Linke, and D. W. Heermann, Thin Solid Films (to be published); D. W. Heermann, A. Linke, G. Pätzold, and T. Hapke, *Deformation of polymer films by bending force*, contribution Ca9.14 to the MRS 1996 fall meeting, December 2-6, Boston, Massachusetts (symposium Ca: structure and evolution of surfaces); `http://wwwcp.tphys.uni-heidelberg.de/~paetzold/`.

[9] M. P. Allen and D. J. Tildesley, *Computer Simulation of Liquids* (Clarendon Press, Oxford, 1987); D. Rigby and R. J. Roe, J. Chem. Phys. **87**, 7285 (1987); Th. Hapke, *Simulation mikromechanischer Eigenschaften von amorphen makromolekularen Gläsern am Beispiel von Polyethylen*, Diplomarbeit am Institut für Theoretische Physik der Universität Heidelberg, 1995.

[10] W. Paul, D. Y. Yoon, and G. D. Smith, J. Chem. Phys. **103**, 1702 (1995).

[11] T. Hapke, A. Linke, G. Pätzold, and D. W. Heermann, Surface Science (to be published); G. Pätzold, D. W. Heermann, A. Linke, and T. Hapke, *Computer studies on free and confined amorphous polymer films*, contribution FF1.4 to the MRS 1996 fall meeting, December 2-6, Boston, Massachusetts (symposium FF: dynamics in small confining systems IV); `http://wwwcp.tphys.uni-heidelberg.de/~paetzold/`.

[12] A. Linke, G. Pätzold, T. Hapke, D. W. Heermann (unpublished).

[13] R. B. Bird, R. C. Armstrong, O. Hassager, and C. F. Curtiss, *Dynamics of Polymeric Liquids*, (Wiley, New York, 1977); M. Doi and S. F. Edwards, *The Theory of Polymer Dynamics* (Clarendon Press, Oxford, 1986).

[14] E. Becker and W. Bürger, *Kontinuumsmechanik* (Teubner-Verlag, Stuttgart, 1975).